

Highly Selective Two-Electron Oxygen Reduction Catalyzed by Mesoporous Nitrogen-Doped Carbon

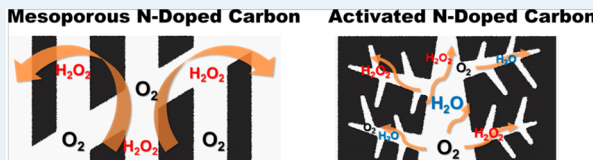
Jisung Park, Yuta Nabae,* Teruaki Hayakawa, and Masa-aki Kakimoto

Department of Organic and Polymeric Materials, Tokyo Institute of Technology, 2-12-1 S8-26, Ookayama, Meguro-ku, Tokyo 152-8552, Japan

Supporting Information

ABSTRACT: Electrochemical reduction of oxygen molecules can produce H_2O_2 , which is an important chemical for a green and sustainable society; therefore, the development of catalysts for this reaction is necessary. We propose mesoporous nitrogen-doped carbon prepared from (1-methyl-1H-pyrrole-2-yl)methanol in the presence of a mesoporous SiO_2 template (KIT-6). The nitrogen content of the resulting carbon can be controlled in the range of 0–10 at. % and all prepared samples have well-ordered mesopores with diameters of 3.4–4.0 nm. Electrochemical studies indicate the present materials have high catalytic activities with high selectivity toward H_2O_2 over 90%. Such high selectivity toward H_2O_2 is probably due to good mass transport in the catalyst layer, which is enhanced by the mesoporous structure.

KEYWORDS: hydrogen peroxide, hard template, carbon catalyst, electrocatalysis, KIT-6



INTRODUCTION

Developing an electrochemical oxygen reduction reaction (ORR) based on a nonprecious metal (NPM) catalyst is very important for the establishment of green and sustainable chemistry. The four-electron reduction pathway produces H_2O and releases a relatively large free energy (1.23 V vs RHE), while the two-electron reduction pathway produces H_2O_2 at a lower potential (0.7 V vs RHE). With the consideration of fuel cell applications, numerous studies have been published regarding NPM catalysts prepared from precursors containing Fe (or Co), C, and N.^{1–6} These catalysts tend to exhibit relatively high electron numbers close to 4, and transition-metal centers such as the FeN_x moiety have been considered to be the active sites for four-electron reduction. However, Olson et al. quite recently proposed that the nominal four-electron reduction actually consists of a 2 + 2 reduction pathway that starts from the two-electron reduction to form H_2O_2 .⁷ Therefore, understanding the nature of 2-electron reduction is important for the design of highly active NPM catalysts for fuel-cell applications. Moreover, the two-electron reduction of oxygen itself includes a very important application, i.e., the electrochemical synthesis of H_2O_2 .⁸ H_2O_2 is a key chemical, especially in the paper industry, and is expected to be increasingly used as an oxidizing agent for green and sustainable chemistry. Instead of the current multistep anthraquinone process, which requires a large amount of energy, direct synthesis of H_2O_2 by the electrochemical reduction of oxygen is receiving much attention, with respect to developing more ecofriendly processes. As such, several cathode catalysts have been proposed for the electrochemical reduction of oxygen,^{9,10} and Co- or Mn-based catalysts are considered to be state-of-the-art catalysts.^{11,12}

Transition-metal centers have been considered to be essential for the ORR; however, several nitrogen-doped carbon materials without transition metals have been reported,^{13–17} although their catalytic performance and selectivity are not as good as the transition-metal-based catalysts. If a highly active metal-free electrocatalyst for the two-electron ORR could be demonstrated, then a more environmentally friendly electrochemical system for H_2O_2 production could be achieved. In addition, useful information could be obtained to further our understanding of the 2 + 2 reduction pathway.

To improve the catalytic activity and control the catalytic selectivity, it is important to control the mesoporous structure of the catalyst material. In this context, mesoporous carbons are promising materials for electrocatalysts. The synthesis of highly ordered mesoporous carbon was first reported in 1999 by Ryoo et al.¹⁸ Ordered mesoporous carbons are typically synthesized from organic carbon sources such as furfuryl alcohol (FFA) in the presence of a hard template such as mesoporous silica.^{19,20} Mesoporous nitrogen-doped carbon (MNC) can be synthesized via similar hard-templating methods by the introduction of nitrogen-containing precursors. Vinu et al. reported the synthesis of MNC from carbon tetrachloride and ethylene diamine, but these precursors are hazardous.²¹ Park et al. reported a synthetic route using the incipient wetness method with cyanamide as a precursor; however, this resulted in a poorly ordered structure because cyanamide did not distribute well in the template.²² Fulvio et al. reported the synthesis of MNC via the chemical vapor infiltration of pyrrole into mesoporous silica and the resulting carbon showed $780\text{ m}^2\text{ g}^{-1}$

Received: June 12, 2014

Revised: August 8, 2014

Published: September 12, 2014



of BET surface area and 3–8 wt % of nitrogen.²³ Fellinger et al. reported the synthesis of MNC with BET surface area of 320 m² g⁻¹ and demonstrated the electrocatalytic activity for H₂O₂ synthesis.²⁴ These pioneering works suggest that the synthesis of well-ordered MNC is slightly more difficult than that of nitrogen-free mesoporous carbon, and there is room for improvement.

In the present study, we propose the use of (1-methyl-1H-pyrrole-2-yl)methanol (MPM), which has a similar chemical structure to furfuryl alcohol, as a new precursor for the production of well-ordered MNCs. Figure 1 shows a schematic

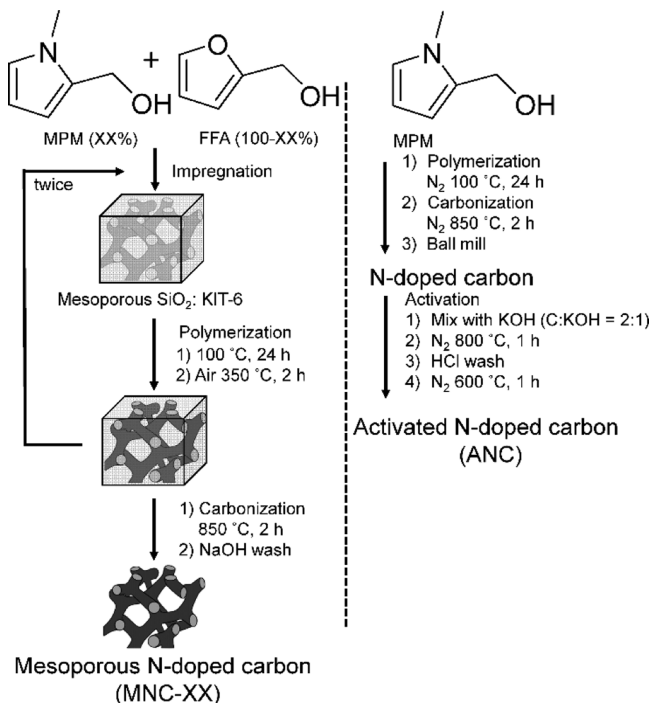


Figure 1. Procedure for the synthesis of mesoporous N-doped carbon and activated N-doped carbon.

of the MNC synthesis procedure. We have successfully synthesized well-ordered mesoporous carbon from MPM in the presence of a mesoporous SiO₂ template (KIT-6), and studied its electrocatalytic activity for ORR in acidic media. Moreover, to discuss the effect of the mesopores in MNC on the catalytic properties, an activated nitrogen-doped carbon (ANC) has also been prepared without the SiO₂ template, and its electrocatalytic activity has been studied.

EXPERIMENTAL SECTION

Synthesis of (1-Methyl-1H-pyrrole-2-yl)methanol.

Twenty grams (20 g) of 1-methyl-1H-pyrrole-2-carboxaldehyde and 10 g of NaBH₄ were added to 500 mL of tetrahydrofuran in a three-necked flask and stirred at room temperature (RT) for 2 h. After the addition of 500 mL of water to dissolve the residual NaBH₄, the mixture was twice extracted with dichloromethane. The organic extracts were washed with water and dried over MgSO₄, and a few drops of triethylamine were added as a stabilizer. The solution was then concentrated with a rotary evaporator. Finally, the yellow liquid was purified by distillation and MPM was collected as a clear colorless liquid. Yield: 80%. ¹H NMR (400 MHz, DMSO, δ, ppm) 3.57 (s, 3H), 4.37 (d, 2H), 4.81 (t, 1H), 5.85 (m, 1H), 5.89 (m, 1H), 6.65 (m, 1H);

¹³C NMR (100 MHz, DMSO, δ, ppm) 33.3, 54.9, 105.8, 107.7, 122.4, 132.6.

Synthesis of Mesoporous Silica, KIT-6.²⁵ In a polypropylene bottle, 8 g of a triblock copolymer (Pluronic P123, Sigma–Aldrich) was dissolved in 300 g of 0.5 M HCl(aq). Eight grams (8 g) of *n*-butanol was added and the solution was stirred at 35 °C for 1 h. Tetraethyl orthosilicate (17.2 g, from Aldrich) was then added and the mixture was stirred continuously at 35 °C for 1 h. The mixture was left to stand at 100 °C for 24 h. After filtration and drying at 100 °C, the obtained powder was washed with a solution of ethanol and HCl to remove the soft template. KIT-6 was finally obtained by calcining the powder at 580 °C for 4 h.

Synthesis of Mesoporous Nitrogen-Doped Carbon.

Four milliliters (4 mL) of a mixture of MPM and furfuryl alcohol (FFA), which corresponds to 80% of the total pore volume of KIT-6, was impregnated into 0.5 g of KIT-6 by the incipient wetness method. The impregnated KIT-6 was heated at 100 °C for 24 h and then at 350 °C for 2 h in air. A quantity of 0.20 mL of the precursor mixture was additionally impregnated into the resulting powder and heated in the same manner. An additional 0.10 mL of the precursor mixture was then impregnated, followed by heating at 100 °C for 24 h, and then at 850 °C for 2 h in a N₂ flow. The resulting powder was washed with a solution of 3 M NaOH in H₂O/EtOH and dried to obtain MNC.

Synthesis of Activated Nitrogen-Doped Carbon. Two grams (2 g) of MPM were heated at 100 °C for 24 h and then at 850 °C for 2 h in a N₂ flow. The resulting powder was ground with a planetary ball mill (Fritsch, P7), physically mixed with KOH (C:KOH = 2:1 w/w) and then heated at 800 °C for 1 h. After washing the mixture with 1 M HCl(aq), the carbon was heated again in a N₂ flow at 600 °C for 1 h.

Characterization. The specific surface area and mesopore volume of the catalysts were determined by N₂ adsorption using a volumetric adsorption instrument (Bel Japan, Belsorp-mini II). The C, H, and N contents of the catalysts were determined using a CHN elemental analyzer (Perkin–Elmer, Model 2400-II). X-ray diffraction (XRD) (Rigaku, Model Ultima IV) was measured at room temperature with Cu Kα radiation. Transmission electron microscopy (TEM) (JEOL, Model 2010F) observations were conducted at an acceleration voltage of 200 kV. X-ray photoelectron spectroscopy (XPS) was performed using a spectrometer (JEOL, Model JPS-9010MC) equipped with a monochromator using an Al anode at 12 kV and 25 mA. The binding energies were charge-corrected, with respect to the C 1s signal at 284.6 eV.

Electrochemical Study. The catalytic activity of the samples was evaluated using linear sweep voltammetry (LSV) (5 mV s⁻¹) with a rotating ring-disk electrode (RRDE).⁵ The catalyst powder was dispersed in a mixture of Nafion solution (5 wt %, Aldrich), ethanol, and water and then was applied to the surface of a glassy carbon electrode. The amount of catalyst loading was 0.2 mg cm⁻². The rotation speed of the RDE was controlled with an RDE system (Nikko Keisoku, RDE-1) and the electrochemical data were collected with a potentiostat (ALS, 2323). LSV was first performed in N₂-saturated H₂SO₄ (0.5 M), and then in O₂-saturated H₂SO₄. The ORR current was determined by subtracting the N₂ current from the O₂ current. The potential of the Pt ring electrode was kept at 1.2 V (RHE) for the detection of H₂O₂ produced on the disk electrode and the selectivity for the two-electron reduction, X(H₂O₂), was calculated using the following equation:

$$X(H_2O_2) (\%) = 2 \times \frac{\frac{j_R}{N}}{j_D + \frac{j_R}{N}} \times 100 \quad (1)$$

where j_D is the disk current, j_R the ring current, and N the collection factor, which was experimentally determined as 0.25 by the redox of Fe^{3+}/Fe^{2+} .

RESULTS AND DISCUSSION

Synthesis and Characterization of Mesoporous Nitrogen-Doped Carbon.

Figure 2 shows X-ray diffraction (XRD)

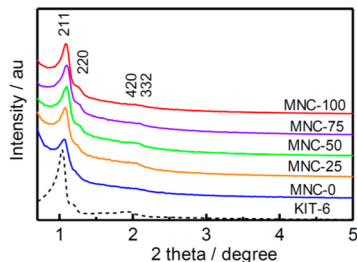


Figure 2. XRD patterns for KIT-6 and MNCs.

patterns for the MNCs, where MNC-X represents the product from a starting mixture of X mol % MPM and $100 - X$ mol % FFA. All MNCs have clear diffraction patterns, similar to that of KIT-6, assigned to the (211) and (220) planes of a cubic mesoporous structure with the $Ia3d$ space group. Figure 3

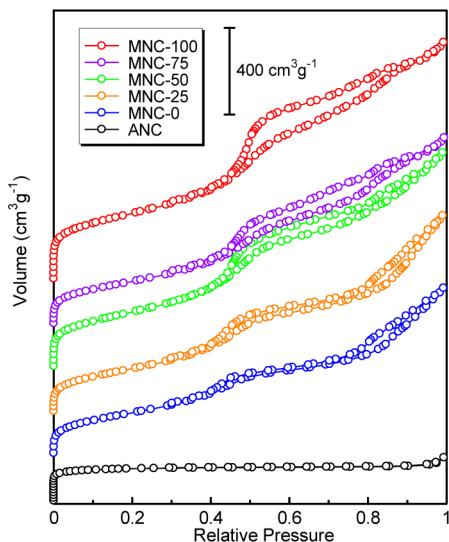


Figure 3. N_2 adsorption isotherms for MNCs and ANC at 77 K.

shows nitrogen adsorption–desorption isotherms for the MNCs, each of which has IUPAC type IV characteristics with a hysteresis loop and two capillary condensation steps in the mesopore range, which indicate the presence of uniform mesopores. The adsorption isotherms were analyzed using the Barrett–Joyner–Halenda (BJH) method and the pore size distributions are shown in Figure 4. All of the MNCs exhibit narrow pore size distributions centered at ~ 3.7 nm. The detailed results of N_2 adsorption are summarized in Table 1. The MNCs have high Brunauer, Emmett and Teller (BET) specific surface areas (S_{BET}) of $780\text{--}1150\text{ m}^2\text{ g}^{-1}$. It should be noted that the mesopore volumes calculated by the BJH

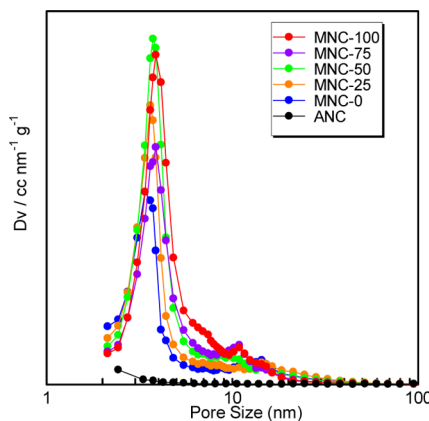


Figure 4. Pore size distribution evaluated by the BJH method for the N_2 adsorption isotherms.

Table 1. Results of N_2 Adsorption and Elemental Analysis

sample	S_{BET} ($m^2\text{ g}^{-1}$)	V_{Total}^a ($mL\text{ g}^{-1}$)	V_{meso}^b ($mL\text{ g}^{-1}$)	V_{Total}/V_{meso}	D_{Pore}^b (nm)	N/C ratio ^c
MNC-00	782	1.21	1.15	0.91	3.4	0.008
MNC-25	799	1.41	1.42	0.95	3.6	0.043
MNC-50	990	1.55	1.53	1.01	3.7	0.069
MNC-75	796	1.33	1.35	0.99	3.9	0.077
MNC-100	1152	1.70	1.64	1.02	3.9	0.099
ANC	616	0.32	0.09	0.27	<2	0.050

^aDetermined from the adsorption volume at $p/p_0 = 0.99$. ^bCalculated using the BJH method. ^cDetermined using elemental analysis

method are very close to the total pore volumes evaluated from the adsorption volumes at $P/P_0 = 0.99$ for all MNC samples. This confirms that this synthesis method can introduce mesoporosity with extremely high selectivity. Figure 5 shows transmission electron microscopy (TEM) images of the MNCs, which indicate that well ordered mesostructures have been introduced into the resulting carbons. Thus, the mesostructure of KIT-6 was successfully transferred to the MNCs. The nitrogen contents of the prepared MNCs were investigated by elemental analysis and the N/C values are shown in Table 1. The results show that the nitrogen content of MNC can be controlled in the range of 0–10 at. % by simply changing the mixing ratio of MPM and FFA.

To discuss the effect of the mesopores in MNC on the catalytic properties, an activated nitrogen-doped carbon (ANC) was also prepared without the SiO_2 template, as shown in Figure 1. The porous structure of ANC was unlike that of the MNCs, although the N/C of 0.050 was similar to those for MNC-50 (Table 1). The N_2 adsorption isotherm for ANC in Figure 3 has IUPAC type I characteristics, which suggests that ANC consists mainly of micropores. The BJH analysis results presented in Figure 4 do not show a clear mesoporous structure for ANC. Therefore, MNC-50 and ANC are a good sample pair to discuss the effect of mesoporous structure, because they have similar nitrogen contents but different porous structures.

The surface properties of MNC-50 and ANC were investigated to clarify the effect of different pyrolysis protocols. Figure 6 shows X-ray photoelectron spectroscopy (XPS) spectra for MNC-50 and ANC. The C 1s spectra can be

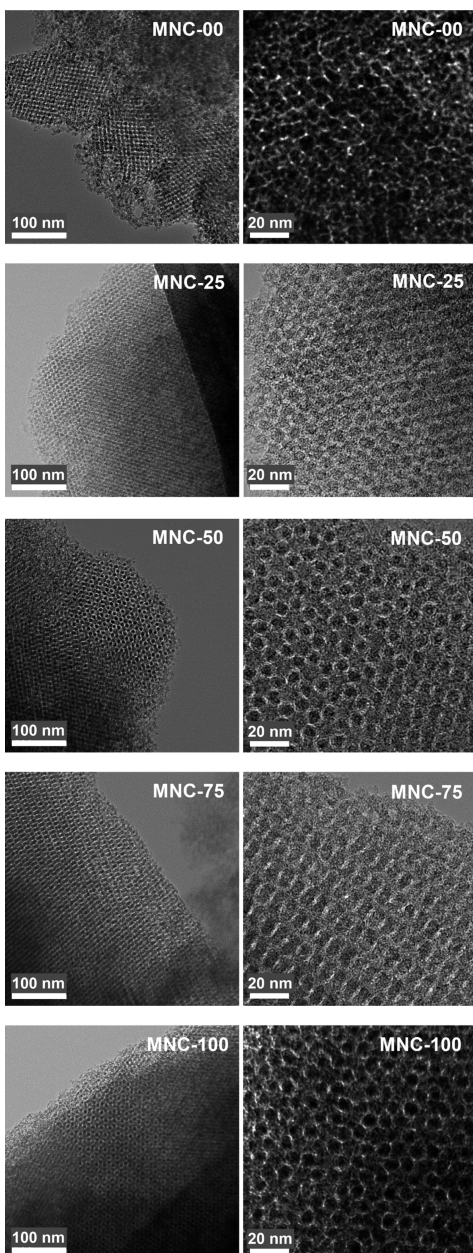


Figure 5. Transmission electron microscopy (TEM) images of mesoporous nitrogen-doped carbon (MNC).

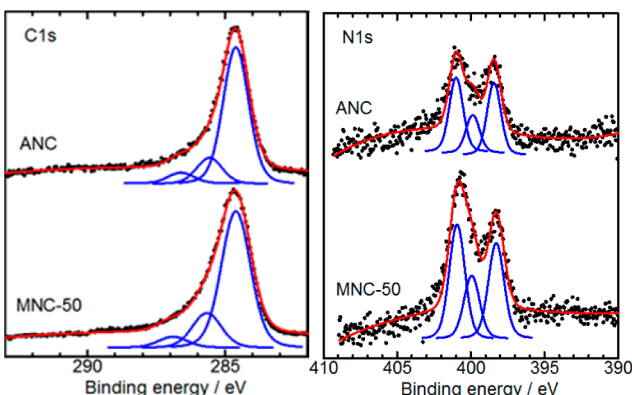


Figure 6. C 1s and N 1s XPS spectra of MNC-50 and ANC.

divided into three peaks by the deconvolution method: aromatic carbon at 284.6 eV, ether (C^*OC) species at 285.6–285.7 eV and ester ($C^*OC=O$) species at 286.6–286.9 eV.²⁶ The N 1s spectra can also be divided into three peaks: pyridinic (398.4–398.5 eV), pyrrolic (399.9–400.0 eV), and graphitic (401.0–401.2 eV).²⁷ The majority of N 1s signals can be assigned to pyridinic and graphitic nitrogen, which have been proposed as catalytically active nitrogen species for the ORR.^{4,28–30} The XPS spectra of MNC-50 and ANC are quite similar; therefore, it can be concluded that their surface properties are similar.

Electrochemical Study. Figure 7 shows RRDE voltammograms for the MNCs and ANC. The ORR current densities are

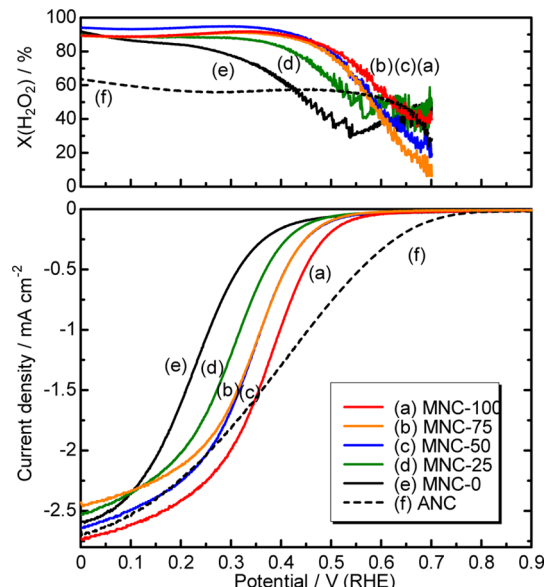


Figure 7. RRDE voltammograms for the ORR with the MNCs and ANC. Conditions: temperature, room temperature (RT); catalyst loading, 0.2 mg cm^{-2} ; electrolyte, $0.5 \text{ M H}_2\text{SO}_4$; rotation, 1500 rpm.

shown as the difference between the N_2 current and O_2 current. (Individual N_2 and O_2 voltammograms are shown in the Supporting Information.) The voltammogram for MNC-0 suggests that it has catalytic activity for the ORR, even if it does not contain any nitrogen species. It is interesting that the ORR curves are shifted toward positive potential as the nitrogen content increased. Pyridinic and graphitic nitrogen are probably responsible for the catalytic activity in ORR, as proposed in the literature.^{4,28–30} Note that the $X(H_2O_2)$ values for the MNCs are extremely high (>90%). To our knowledge, this two-electron reduction performance is better than that of state-of-the-art metal-free catalyst. Table 2 summarizes the ring currents and formation rates of H_2O_2 , which was calculated from the ring current, with MNCs and ANC at 0.4 and 0.1 V (RHE). At 0.1 V, MNC-100 exhibits a ring current of 0.148 mA , which corresponds to H_2O_2 formation at 3.06 pmol s^{-1} , while Fellinger et al. reported 2.13 pmol s^{-1} of H_2O_2 formation over the BMP-800 catalyst using a similar experimental setup.²⁴ This is probably because the MNC-100 has a higher specific surface area ($1152 \text{ m}^2 \text{ g}^{-1}$) than BMP-800 ($320 \text{ m}^2 \text{ g}^{-1}$). Moreover, this performance is comparable with that for transition-metal-based catalysts. MNC-100 exhibits a ring current of 0.057 mA at 0.4 V (RHE) and 1500 rpm, which corresponds to H_2O_2 formation at 1.18 pmol s^{-1} , while Yamanaka et al. reported ring currents of

Table 2. Ring Current Values and Formation Rates of H_2O_2 with MNCs and ANC at 0.4 and 0.1 V (RHE) under 1500 rpm

sample	j_R (μA)		$r(\text{H}_2\text{O}_2)^a$ (pmol s^{-1})	
	0.4 V	0.1 V	0.4 V	0.1 V
MNC-100	57	148	1.18	3.06
MNC-75	33	138	0.68	2.86
MNC-50	35	154	0.72	3.19
MNC-25	15	132	0.31	2.74
MNC-0	5	127	0.11	2.63
ANC	42	81	0.88	1.68

$$^a r(\text{H}_2\text{O}_2) = j_R / (2NF)$$

~0.15 and 0.02 mA for Co- and Mn-based catalysts, respectively, using a similar experimental setup.^{11,12} It is significant that such a two-electron reduction performance has been achieved with a metal-free carbon catalyst in the present work. In contrast to MNCs, the micropore-dominant ANC (Table 1) shows a higher onset potential than MNC-50 and a lower $X(\text{H}_2\text{O}_2)$ value, although they are still quite different from those with state-of-the-art Pt-based catalysts, which shows an onset potential over 1 V and no H_2O_2 formation.^{31,32}

The selectivity values toward H_2O_2 over MNC-50 and ANC were double-checked by preparing Koutecky–Levich (KL) plots. RRDE voltammetry was performed at 100, 400, 900, 1600, and 2500 rpm and $1/j_D$ is plotted against $\omega^{-1/2}$ in Figure 8, where ω

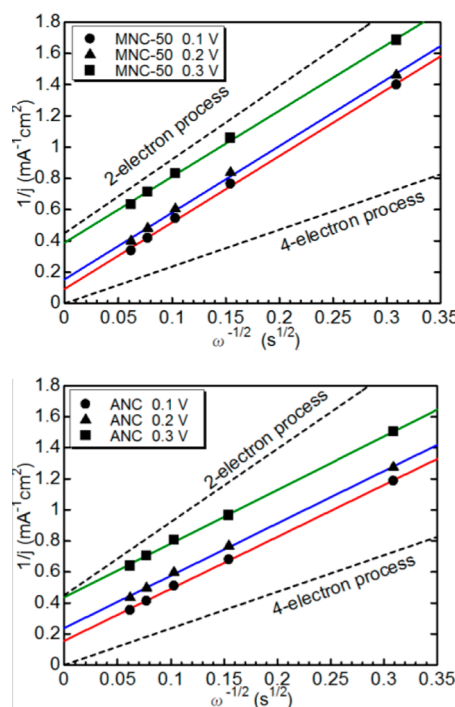


Figure 8. Koutecky–Levich (KL) plots for MNC-50 and ANC.

is the rotation speed of the electrode. The slope of the KL plot for MNC-50 is very close to the theoretical slope for 2-electron reduction. In contrast, ANC has a lower slope, which indicates a higher electron number for the ORR. The slopes were converted to $X(\text{H}_2\text{O}_2)$, using the following equations:

$$B = 0.62zFD^{2/3}\nu^{-1/6}C \quad (2)$$

$$X(\text{H}_2\text{O}_2) (\%) = \left(2 - \frac{z}{2} \right) \times 100 \quad (3)$$

where B is the slope of the KL plot, z the electron number of the ORR, F the Faraday constant ($96\,485 \text{ C mol}^{-1}$), D the diffusion coefficient for oxygen ($1.36 \times 10^{-5} \text{ cm}^2 \text{ s}^{-1}$), ν the kinetic viscosity ($1.0 \times 10^{-2} \text{ cm}^2 \text{ s}^{-1}$), and C the bulk concentration of O_2 ($1.49 \times 10^{-6} \text{ mol cm}^{-2}$).³³ Table 3

Table 3. Selectivity toward Two-Electron Reduction Evaluated from Koutecky–Levich (KL) Plots and RRDE Voltammetry

resource	Selectivity (%)					
	MNC-50			ANC		
	0.1 V	0.2 V	0.3 V	0.1 V	0.2 V	0.3 V
KL plot	93	93	92	58	62	70
RRDE	93	94	95	60	57	56

presents a comparison of the $X(\text{H}_2\text{O}_2)$ values determined from RRDE voltammetry and the KL plots. These results are in good agreement with MNC-50 showing high $X(\text{H}_2\text{O}_2)$ values over 90%, whereas ANC has lower values.

The extremely high selectivity of the MNCs toward the two-electron pathway can be explained as illustrated in Figure 9.

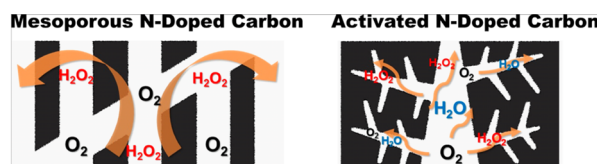


Figure 9. Schematic images of the oxygen reduction reaction (ORR) over (left) mesoporous carbon catalysts and (right) microporous carbon catalysts.

The ORR on the nitrogen-doped carbon surface probably starts with two-electron reduction to form H_2O_2 . In the case of mesoporous catalysts, the H_2O_2 produced can be released within a relatively short contact time, because of the ease of mass transport; therefore, H_2O_2 can be produced with extremely high selectivity. In contrast, H_2O_2 produced in the micropore-dominant ANC is resident for a longer time and, thus, has a greater chance to be further reduced to form H_2O or decompose by disproportionation; therefore, the ORR results in a lower selectivity toward H_2O_2 . This tendency will become stronger if a catalyst contains some transition metals such as Fe, which increases the electron number of ORR; Xu et al. reported very high electron numbers (3–4) with a Fe–N–C-based catalyst, despite its mesoporous structure.³⁴ In other words, another criterion, as well as mesoporous structure, to achieve an extremely high selectivity toward H_2O_2 is to avoid active centers that increase the electron number and it could be stated that, with regard to this aspect, nitrogen-doped carbon without transition metals is a suitable material.

CONCLUSION

Highly ordered mesoporous nitrogen-doped carbon materials have been successfully synthesized. These materials exhibit excellent catalytic activities for electrochemical oxygen reduction to produce H_2O_2 . Comparison of the mesopore-dominant nitrogen-doped carbon and a micropore-dominant nitrogen-doped carbon suggests that the mesoporous structure

enhances mass transport in the catalyst layer, which results in an extremely high selectivity toward H_2O_2 . Further studies are planned in order to clarify the detailed reaction mechanism and to further develop active ORR catalysts.

■ ASSOCIATED CONTENT

Supporting Information

RDE voltammograms with N_2 and O_2 are provided as Supporting Information. This material is available free of charge via the Internet at <http://pubs.acs.org>.

■ AUTHOR INFORMATION

Corresponding Author

*E-mail: nabae.y.aa@m.titech.ac.jp.

Notes

The authors declare no competing financial interest.

■ ACKNOWLEDGMENTS

The authors thank Prof. Ryong Ryoo for valuable assistance in the mesoporous carbon synthesis. The TEM measurements were performed in the Center for Advanced Materials Analysis in Tokyo Institute of Technology. M.K. was supported by Visiting Professorship for Senior International Scientists from Chinese Academy of Science.

■ REFERENCES

- (1) Jahnke, H.; Schönborn, M.; Zimmermann, G. *Top. Curr. Chem.* **1976**, *61*, 133–181.
- (2) Proietti, E.; Jaouen, F.; Lefevre, M.; Larouche, N.; Tian, J.; Herranz, J.; Dodelet, J. P. *Nat. Commun.* **2011**, *2*, 416.
- (3) Wu, G.; More, K. L.; Johnston, C. M.; Zelenay, P. *Science* **2011**, *332*, 443–447.
- (4) Matter, P. H.; Zhang, L.; Ozkan, U. S. *J. Catal.* **2006**, *239*, 83–96.
- (5) Nabae, Y.; Sonoda, M.; Yamauchi, C.; Hosaka, Y.; Isoda, A.; Aoki, T. *Catal. Sci. Technol.* **2014**, *4*, 1400–1406.
- (6) Nabae, Y.; Kuang, Y.; Chokai, M.; Ichihara, T.; Isoda, A.; Hayakawa, T.; Aoki, T. *J. Mater. Chem. A* **2014**, *2*, 11561.
- (7) Olson, T. S.; Pylypenko, S.; Fulghum, J. E.; Atanassov, P. *J. Electrochem. Soc.* **2010**, *157*, B54–B63.
- (8) Yamanaka, I.; Onizawa, T.; Takenaka, S.; Otsuka, K. *Angew. Chem., Int. Ed.* **2003**, *42*, 3653–3655.
- (9) Jirkovský, J. S.; Panas, I.; Ahlberg, E.; Halasa, M.; Romani, S.; Schiffriin, D. *J. Am. Chem. Soc.* **2011**, *133*, 19432–19441.
- (10) Siahrostami, S.; Verdaguer-Casadevall, A.; Karamad, M.; Deiana, D.; Malacrida, P.; Wickman, B.; Escudero-Escribano, M.; Paoli, E. A.; Frydendal, R.; Hansen, T. W.; Chorkendorff, I.; Stephens, I. E. L.; Rossmeisl, J. *Nat. Mater.* **2013**, *12*, 1137–1143.
- (11) Yamanaka, I.; Ichihashi, R.; Iwasaki, T.; Nishimura, N.; Murayama, T.; Ueda, W.; Takenaka, S. *Electrochim. Acta* **2013**, *108*, 321–329.
- (12) Yamanaka, I.; Onizawa, T.; Suzuki, H.; Hanaizumi, N.; Nishimura, N.; Takenaka, S. *J. Phys. Chem. C* **2012**, *116*, 4572–4583.
- (13) Gong, K. P.; Du, F.; Xia, Z. H.; Durstock, M.; Dai, L. M. *Science* **2009**, *323*, 760–764.
- (14) Lee, Y.-H.; Li, F.; Chang, K.-H.; Hu, C.-C.; Ohsaka, T. *Appl. Catal., B* **2012**, *126*, 208–214.
- (15) Iwazaki, T.; Obinata, R.; Sugimoto, W.; Takasu, Y. *Electrochim. Commun.* **2009**, *11*, 376–378.
- (16) Chokai, M.; Taniguchi, M.; Moriya, S.; Matsubayashi, K.; Shinoda, T.; Nabae, Y.; Kuroki, S.; Hayakawa, T.; Kakimoto, M.; Ozaki, J.; Miyata, S. *J. Power Sources* **2010**, *195*, 5947–5951.
- (17) Wei, W.; Liang, H.; Parvez, K.; Zhuang, X.; Feng, X.; Müllen, K. *Angew. Chem., Int. Ed.* **2014**, *53*, 1570–1574.
- (18) Ryoo, R.; Joo, S. H.; Jun, S. *J. Phys. Chem. B* **1999**, *103*, 7743–7746.
- (19) Fuertes, A. B. *J. Mater. Chem.* **2003**, *13*, 3085–3088.
- (20) Kim, T.-W.; Ryoo, R.; Gierszal, K. P.; Jaroniec, M.; Solovyov, L. A.; Sakamoto, Y.; Terasaki, O. *J. Mater. Chem.* **2005**, *15*, 1560–1571.
- (21) Vinu, A.; Ariga, K.; Mori, T.; Nakanishi, T.; Hishita, S.; Golberg, D.; Bando, Y. *Adv. Mater.* **2005**, *17*, 1648–1652.
- (22) Park, S. S.; Chu, S.-W.; Xue, C.; Zhao, D.; Ha, C.-S. *J. Mater. Chem.* **2011**, *21*, 10801–10807.
- (23) Fulvio, P. F.; Jaroniec, M.; Liang, C.; Dai, S. *J. Phys. Chem. C* **2008**, *112*, 13126–13133.
- (24) Fellinger, T.-P.; Hasché, F.; Strasser, P.; Antonietti, M. *J. Am. Chem. Soc.* **2012**, *134*, 4072–4075.
- (25) Kim, T.-W.; Kleitz, F.; Paul, B.; Ryoo, R. *J. Am. Chem. Soc.* **2005**, *127*, 7601–7610.
- (26) Desimoni, E.; Casella, G. I.; Morone, A.; Salvi, A. M. *Surf. Interface Anal.* **1990**, *15*, 627–634.
- (27) Raymundo-Pinero, E.; Cazorla-Amoros, D.; Linares-Solano, A.; Find, J.; Wild, U.; Schlogl, R. *Carbon* **2002**, *40*, 597–608.
- (28) Kuroki, S.; Nabae, Y.; Chokai, M.; Kakimoto, M.; Miyata, S. *Carbon* **2012**, *50*, 153–162.
- (29) Ikeda, T.; Boero, M.; Huang, S. F.; Terakura, K.; Oshima, M.; Ozaki, J. *J. Phys. Chem. C* **2008**, *112*, 14706–14709.
- (30) Sidik, R. A.; Anderson, A. B.; Subramanian, N. P.; Kumaraguru, S. P.; Popov, B. N. *J. Phys. Chem. B* **2006**, *110*, 1787–1793.
- (31) Tiwari, J. N.; Nath, K.; Kumar, S.; Tiwari, R. N.; Kemp, K. C.; Le, N. H.; Youn, D. H.; Lee, J. S.; Kim, K. S. *Nat. Commun.* **2013**, *4*, 2221.
- (32) Tiwari, J. N.; Kemp, K. C.; Nath, K.; Tiwari, R. N.; Nam, H.-G.; Kim, K. S. *ACS Nano* **2013**, *7*, 9223.
- (33) Castellanos, R. H.; Ocampo, A. L.; Sebastian, P. J. *J. New Mater. Electrochem. Systems* **2002**, *5*, 83–90.
- (34) Yan, X.-H.; Xu, B.-Q. *J. Mater. Chem. A* **2014**, *2*, 8617.